PULSE WAVE REFLECTIONS IN BRANCHING ARTERIAL NETWORKS AND PULSE DIAGNOSIS METHODS

Natalya N. Kizilova

ABSTRACT

Wave propagation and reflection in the model of branching tree of viscoelastic cylindrical tubes filled with viscous fluid is considered when applied to pulse wave reflection in arterial networks. The dichotomous branching tree and the tree with two anastomoses between the second-order tubes are investigated. Influence of the geometrical and mechanical properties of the tree on the pulse wave propagation and spectral properties of the total admittance of the systems are investigated. It was found out that the admittance has a set of resonant harmonics. Any changes in parameters of microcirculatory bed and in blood rheology cause noticeable alterations of the amplitudes of resonant harmonics and negligible alterations of other harmonics. The set of resonant harmonics is independent of some variations in the tree geometry. The resonant properties of the models with and without anastomoses have some differences, that makes it possible to carry out the diagnosis of the state of inner organs with different types of vasculature. The results substantiate a possibility of the pulse diagnosis of inner organs' states by observing the amplitudes of the resonant harmonics only, without preliminary knowledge of individual structure of the real vascular bed of an inner organ.

Key Words: pulse wave reflections, pulse diagnosis, cardiovascular system, branching transport networks.

I. INTRODUCTION

Understanding of blood motion and pulse wave propagation in cardiovascular system is a very important step for investigation of blood pressure regulation, normal and pathological state differences, and mechanisms of pathology state formation. Such hemodynamic parameters as pulse rate, pulse pressure and pulse wave velocity are widely used in medical diagnosis. The biomechanical models help us to understand the physical sense of the measured physiological parameters and to interpret their values for treatment purposes. The models must take into consideration the pulsatile character of blood motion, vessel wall properties, blood rheology and vessels' system geometry (Milnor, 1989).

The arterial system is a complicated irregular branching system of elastic vessels, whose mechanical and geometrical properties differ in different inner organs. Morphometric data on lengths, diameters, branching angles and number of vessels of consecutive branching orders were obtained for pulmonary arterial and venous (Huang *et al.*, 1996; Gan *et al.*, 1993; Dawson *et al.*, 1999) coronary (Zamir and Shee, 1985; 1987; Aharinejad *et al.*, 1998) and renal arterial tree casts (Gil-Garcia *et al.*, 1992; Cross *et al.*, 1995; Zamir and Phipps, 1987). The tree morphology is tightly connected with the organ form, size and function. In spite of the individual variations in tree structure a number of parameters such as fractal dimension, branching coefficients, asymmetry coefficients are rather constant for a given organ from a statistical viewpoint. Morphometric analysis has revealed some regularities in the tree organization. A satisfactory accordance of the tree geometry to the model of an optimal branching pipeline was found, that provides the uniform delivery of the transported fluid to the system of distributed consumers (alive

N. N. Kizilova is with the Kharkov National University, 4 Svobody sq., 61077, Kharkiv, Ukraine. (Email: knn@hall.nord.net.ua)

cells) at minimum total cost at a given total volume of the transport system. The averaged parameters are used in continual models of the transport systems of inner organs (Dawson *et al*., 1999) whereas the precise data are used in discrete tree models (Zamir, 1998; 2001).

The pulse wave gets into the organ by the feeding artery that is usually the largest one in the tree. Each arterial bifurcation as well as the difference in the mechanical and geometrical properties of the consecutive vessels, both narrowing and widening of the vessels produce the backward wave. The superposition of the forward and backward waves forms the pressure and flow oscillations in the vessels. Due to the superposition the pressure and flow waves change in shape and size as they travel through the arterial system. The elasticity of the arterial walls is responsible for transforming the oscillatory cardiac outflow into a relatively steady blood flow in peripheral vessels. During the cardiac cycle the diameters of the vessels vary rhythmically, they can be palpated on any superficial peripheral artery.

The unique method of pulse diagnosis of traditional Chinese medicine gives an accurate and sensible tool for the early diagnosis of the whole organ state, its regulatory systems and inner organ diseases, treatment prescribing, disease correction and prevention. Palpating the pulse of the radial arteries at the wrists and at other sites around the body is connected with consecutive compressions of the arteries and some pulse parameters estimation (Hammer, 2001; Wang, 1997; Flaws, 1997). Computer assisted pulse detection devices help to obtain pulse wave curves, to calculate a series of parameters (pulse contour analysis) and Fourier spectrum of the signal (spectral analysis of the pulse wave). A reasonable biomechanical interpretation of the pulse pressure method, more particularly the inner organ state diagnosis is absent at the moment.

Recent investigations have offered a new pulse diagnosis method that is based on the concept of the so-called resonant frequencies (Wang *et al*., 1991). Both experimental investigations and clinical observations have revealed the existence of unique sets of resonant frequencies in the Fourier spectrum of the pulse in the inner organs (kidneys, liver, spleen and gall bladder (Yu *et al*., 1994; Lu *et al*., 1996; Young *et al*., 1992; Wang *et al*., 2000a)). The amplitudes of the resonant harmonics depend on the organ state (normal or pathological) and show the state in excess-deficiency terms.

The necessary parameters of the pulse can be estimated on any peripheral artery with a cuff manometer. The main resonant frequency is connected with the length of the feeding artery of the organ's arterial system (Wang *et al*., 2000b). The pressure and flow waves depend on the wave reflection character and, thus, on geometrical and mechanical properties of the arterial system. The biomechanical models of pulse wave propagation and reflection were minutely investigated on the dichotomous branching tree models of the arterial system (Taylor, 1966; Brown, 1996; Bennett, 1996; Bondarenko and Kizilova, 2002). The real vascular networks have numerous anastomoses between the vessels of the same order and differ from the tree models. The pressure distribution and pulse wave propagation in a simple loop (Duan and Zamir, 1993) and in a branching tree with a single anastomos (Kizilova, 2002) exhibit some new properties concerning the resonant harmonics. The arterial trees of some inner organs are similar to the tree model without anastomoses (heart, kidneys, lung, liver) whereas some organs possess arterial systems either with a few anastomoses between the second-order vessels (stomach, tongue, gall bladder) or numerous anastomoses between vessels of equal orders (large and small intestine). The peculiar properties of pressure and flow wave propagation in the arterial systems with and without anastomoses may underlie the differences in Fourier spectra and resonant harmonics of the so-called solid (Yin-Tsang) and hollow (Yang-Fu) organs. In the present study the comparative analysis of pulse pressure propagation and reflection in the two models of branching arterial systems is provided.

II. BIOMECHANICAL MODEL

The biomechanical model used here is based on Womersley's theory (Womersley, 1957). The fluid flow in each tube is described by linearized Navier-Stokes equations. Nonlinear arterial properties are neglected, because in spite of the arterial system nonlinearity, the linear viscoelastic Womersley model describes the pressure wave propagation satisfactorily (Reuderink *et al*., 1989), though observed scatter in spectra of aortic and other elastic type vessels impedance is considered as being produced by nonlinear properties of arterial wall (Stergiopulos *et al*., 1995).

The vasculature of an inner organ without anastomoses is modeled as a set of bifurcated tubes with four orders of branching (model I). Each vessel in it is considered as a viscoelastic thin tethered tube with radius R_i, length L_i and wall thickness h_i, where i is the serial number of the vessel (Fig. 1a). The last-order vessels are terminated in admittances Y_i^t (or impedances $Z_i^t = (Y_i^t)^{-1}$), that are complex numbers and represent the peripheral load (arteriolar and capillary levels of branching). The values $\mathrm{Re}(Y_i^t)$ and $\mathrm{Im}(Y_i^t)$ determine the amplitudes and phases of the backward waves and correspond to the hemodynamical state of

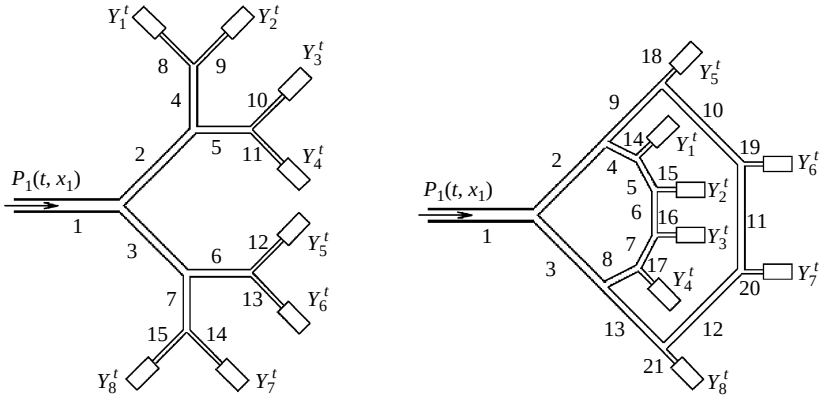

Fig. 1 A multibranched fourth-order model of the inner organ vasculature. (a) dichotomically branching tree; (b) the system with two anastomoses between two second-order vessels

the organ. The influence of the branching angle on the backward wave is not taken into account in this paper because of its relatively small effect (Milnor, 1989). Validation studies of the model used here have demonstrated an excellent agreement with experimental results both for arterial systems and trees of latex tubes (Avolio, 1980; Milnor, 1989).

The second model (Fig. 1b) represents the vasculature with two anastomoses between the second-order vessels (model II). Arterial systems of some hollow organs as well as high and low extremities and tongue possess this kind of vascular topology. In both models each last-order vessel is terminated in the admittance Y_i^t. The total numbers of the terminations are equal in the models. For the purpose of the comparative study the equality of the corresponding admittances Y_i^t (case 1) and the total volumes of the vascular systems for both models (case 2) are assumed. As a result the two models possess different total hydraulic admittances for a steady flow. This approach allows investigation of the influence of vasculature topology only on pulse wave propagation and reflection. Real vascular systems with and without anastomoses possess quite different terminations as well, that correspond to the complicated geometry of the downstream vascular bed either a tree-like structure or a structure with numerous loops.

Both models are valid for using with real morphometric data $\{L_i, R_i\}_i$, $\{Y_k^t\}_k$ of a particular inner organ, where i and k are numbers of tubes and terminations in the model. There are detailed data on pulmonary arterial tree structures including more than 15 branching orders (Huang *et al.*, 1996; Gan *et al.*, 1993; Dawson *et al.*, 1999) which can be used for precise calculations. The terminate admittances can be calculated being based on the data for tubes with branching orders $k>4$ using the scheme that is shown below.

The cylindrical coordinate system (r, φ, x) was connected with the vessels so that $x_i \in [0, L_i]$ is the longitudinal coordinate for the tube number i. It is suggested that pressure and flow continuity conditions are valid for each bifurcation of a parent vessel i and daughter vessels j, k in form:

$$P_i(t, L_i)=P_j(t, 0)=P_k(t, 0)$$

$$Q_i(t, L_i)=Q_j(t, 0)+Q_k(t, 0) \qquad (1)$$

where $Q_{i,j,k}$ - the volumetric rate in the corresponding vessel. At the point of entry to the system $x_1=0$ the pressure wave $P_1(t, 0)=P_1^0 e^{i\omega t}$ is given. The parameters P_1^0 and ω are defined by the state of heart and large vessels (aorta and its main branches) and their possible pathological changes are not considered in the present paper. The linear biomechanical model described here is an analogue of the uniform transmission line and corresponding electrical models for different vessels and terminations have been proposed (Milnor, 1989).

III. MORPHOMETRIC DATA

Geometrical parameters $\{L_i, R_i\}_{i=1}^{15}$ and $\{L_i, R_i\}_{i=1}^{21}$ of the two models can be obtained for a given vasculature. For general analysis some regularities in vascular geometry of inner organs were used. Based on statistical morphometric data on branching vascular trees construction (Huang *et al.*, 1996; Dawson *et al.*, 1999; Zamir and Shee, 1985; Aharinejad *et al.*, 1998; Gil-Garcia *et al.*, 1992; Cross *et al.*, 1995) the dependences between the diameters and lengths of the consecutive vessels can be introduced in the following form:

$$R_j = \frac{\xi R_i}{\sqrt[\gamma]{1+\xi^\gamma}}, \quad R_k = \frac{R_i}{\sqrt[\gamma]{1+\xi^\gamma}}$$

$$L_j = \frac{\zeta L_i}{\sqrt[\gamma]{1+\zeta^\gamma}}, \quad L_k = \frac{L_i}{\sqrt[\gamma]{1+\zeta^\gamma}} \tag{2}$$

where i, j, k - are indexes for a parent, smaller and larger daughter vessels respectively; $\xi=R_j/R_k$ and $\zeta=L_j/L_k$ - branching asymmetry coefficients. The variation in parameters ξ, ζ allows obtaining realistic computational models of different inner organs vasculatures (Zamir, 2001). In the framework of continual modeling the relation $L_i=aD_i^b$ is accepted for each arterial segment (Dawson *et al.*, 1999). Most data obtained from plastic casts of the pulmonary vasculature give a=2.6–7.59 for mammals, a=3.57–5.13 for human and b=0.84–1.16 for mammals and human. The values $R_{i,j,k}$ in form (2) obey Murrray's law $R_i^\gamma=R_j^\gamma+R_k^\gamma$, where $\gamma \sim 2.33$ for large elastic vessels (aorta, pulmonary artery), $\gamma \sim 2.92$ for small vessels in which blood rheology is important and the Fareus-Lindqvist effect takes place, γ=1.6–3.02 for most mammalian vascular and respiratory systems (Huang *et al.*, 1996; Dawson *et al.*, 1999; Zamir and Shee, 1985; 1987). On the average γ=3 is chosen as a rule. Then from Murray's law and (2) it follows:

$$\zeta = \frac{\xi^b}{\sqrt[\gamma]{(1+\xi^\gamma)^b - \xi^{\gamma b}}}$$

For a system of proportional scale-independent tubes b=1 and hence it follows $\zeta=\xi$. Asymmetry coefficient is widely used for approaching representation of the vasculature (Zamir and Shee, 1985; 1987; Zamir, 1998). If ζ and ξ do not depend on the vessel number, a uniform model of the vasculature can be built.

For the geometrical identity of the two models considered here the vessels with numbers i=1, 2, 3 (Figs. 1a-b) have the same lengths and radiuses for both models; the vessels i=8–15 of the model I are equal to the vessels i=14–21 of the model II; the vessels i=4–7 of the model I have the same total volume as the vessels i=4–13 of the model II. Based on (2) hence it follows:

a) $\frac{R_5}{R_4}=\frac{R_6}{R_5}=\frac{R_7}{R_6}=\frac{R_8}{R_7}=\frac{R_{10}}{R_9}=\frac{R_{11}}{R_{10}}=\frac{R_{12}}{R_{11}}=\frac{R_{13}}{R_{12}}=\xi^{-1/4}$

at $\frac{R_9}{R_4}=\frac{R_{13}}{R_8}=\xi$

b) $\frac{R_{10}}{R_9}=\frac{R_{11}}{R_{10}}=\frac{R_{12}}{R_{11}}=\frac{R_{13}}{R_{12}}=\xi^{-1/4}$

$R_4=R_5=R_6=R_7=R_8$ at $\frac{R_9}{R_4}=\frac{R_8}{R_{13}}=\xi$

The cases (a) and (b) correspond to the monotonous diminishing of the radius of the compound tubes 4–8 and 9–13 (model II) in the same or in the opposite directions respectively. In the case (a) the total volume V_{8-15} of the tubes with numbers i=8–15 of model I is equal to the corresponding total volume V_{14-21} for the model II at $\zeta=\xi^{-2}$. In the case (b) the chains of tubes i=4–8 and i=9–13 have different branching asymmetry at $\xi\neq1$ (monotonously decreasing radius of the compound tube i=9–13 and uniform tube i=4–8). For the symmetrical bifurcating vasculature with $\xi=\zeta=1$ both the cases coincide.

In the present study γ=3, b=1, were assumed according to the work Dawson *et al*. (1999).

IV. METHODS OF COMPUTATION

Womersley's model of the wave motion of a viscous incompressible liquid in a viscoelastic tube gives for pressures $P_i(t, x_i)$ and volumetric rates $Q_i(t, x_i)$ in tube i (Womersley, 1957; Milnor, 1989; Zamir, 1998):

$$P_i(t, x_i)=P_i^0(e^{i\omega(t-x_i/c_i)}+\Gamma_i e^{i\omega(t+(x_i-2L_i)/c_i)}) \tag{3}$$

$$Q_i(t, x_i)=Y_i^0P_i^0(e^{i\omega(t-x_i/c_i)}-\Gamma_i e^{i\omega(t+(x_i-2L_i)/c_i)}) \tag{4}$$

where $c_i=(\frac{E_ih_i(1-F_{01})}{2\rho R_i(1-\sigma_i^2)}e^{I\theta_i})^{1/2}$, $I=\sqrt{-1}$, $P_i^0=P_i\big|_{x_i=0}$, $F_i=2J_1(\beta_i)/(\beta_iJ_0(\beta_i))$, $\beta_i=\alpha_i(-1)^{3/4}$, $\alpha_i=R_i\sqrt{\omega\rho/\mu}$ – Womersley's number, $Y_i^0=(\pi R_i^2)/(\rho c_i)$ - characteristic admittance of the tube. In general, Γ_i are the complex values and $\Gamma_i=P_b/P_f$. Each tube is regarded as uniform so that the terminating bifurcation is the only reflecting place in it.

Pressure and flow inside the tube is a result of superimposing of the forward and backward pulse waves. In the absence of wave reflections the admittance depends on the properties of the tube only and is called characteristic admittance Y_i^0 (Milnor, 1989). Backward wave causes diverse pressure and flow wave changes. At the presence of the backward pulse wave the flow-to-pressure ratio at the system's entrance $Y_i=(Q_i/P_i)|_{x_i=0}$ depends on the tube properties and the frequency of the oscillations as well and is called input admittance (Milnor, 1989).

The input admittance Y_1 of both models is defined from (3)-(4) as

$$Y_1 = Y_1^0\frac{1-\Gamma_1e^{-2I\omega L_1/c_1}}{1+\Gamma_1e^{-2I\omega L_1/c_1}} \tag{5}$$

The reflection coefficient Γ_1 depends on the downstream vasculature properties that significantly differ in both models. The general scheme for computating the input admittance of the bifurcating

tree was presented in the work Taylor (1966). The calculations for a given value ω and terminations Y_{1-8}^t begin by finding $Y_i^/$ of the last-order tubes i=8–15 from the formula:

$$Y_i^/ = Y_i^0 \frac{Y_{i-7}^t + iY_i^0 \tan(\omega L_i/c_i)}{Y_i^0 + iY_{i-7}^t \tan(\omega L_i/c_i)}, \quad \Gamma_i = \frac{Y_i^0 - Y_{i-7}^t}{Y_i^0 + Y_{i-7}^t} \quad (6)$$

where i=8–15. By this way the terminations for the tubes number i=4–7 may be represented as parallel connections of the complex admittances $Y_{2i}^/$ and $Y_{2i+1}^/$. Then the complex values $Y_{2i}^/ + Y_{2i+1}^/$, where i=4–7 are considered as the terminal admittances for the tubes i=4–7 and the relations for input admittances $Y_{4-7}^/$ are defined by

$$Y_i^/ = Y_i^0 \frac{Y_{2i}^/ + Y_{2i+1}^/ + iY_i^0 \tan(\omega L_i/c_i)}{Y_i^0 + i(Y_{2i}^/ + Y_{2i+1}^/)\tan(\omega L_i/c_i)}$$

$$\Gamma_i = \frac{Y_i^0 - Y_{2i}^/ - Y_{2i+1}^/}{Y_i^0 + Y_{2i}^/ + Y_{2i+1}^/} \quad (7)$$

In a similar manner the terminations for the tubes number i=2–3 are parallel connections of the complex admittances $Y_{2i}^/$ and $Y_{2i+1}^/$. Two last steps in the calculating procedure consist of applying (7) at i= 2, 3 and i=1 for obtaining $Y_{2-3}^/$ and then $Y_1^/$ consequently.

The same relations are valid for the linear transmission line with complex impedances. In this way the model I can be considered as a single tube number i=1 terminated with the complex admittance that is defined by the repetitive procedure from (6)-(7).

The iterative scheme is not valid for the tree with anastomoses (model II) because of the variety of ways for the backward waves to travel throughout the vasculature. In this case the equations of pressure continuity and flow conservation in each junction have to be considered. For the model II the corresponding system of equations is

$$P_1(t, L_1)=P_2(t, 0)=P_3(t, 0)$$

$$Q_1(t, L_1)=Q_2(t, 0)+Q_3(t, 0)$$

$$P_2(t, L_2)=P_4(t, 0)=P_9(t, 0)$$

$$Q_2(t, L_2)=Q_4(t, 0)+Q_9(t, 0)$$

$$P_3(t, L_3)=P_8(t, L_8)=P_{13}(t, L_{13})$$

$$Q_3(t, L_3)+Q_8(t, L_8)+Q_{13}(t, L_{13})=0$$

$$P_9(t, L_9)=P_{10}(t, 0)=P_{18}(t, 0)$$

$$Q_9(t, L_9)=Q_{10}(t, 0)+Q_{18}(t, 0)$$

$$P_{10}(t, L_{10})=P_{11}(t, 0)=P_{19}(t, 0)$$

$$Q_{10}(t, L_{10})=Q_{11}(t, 0)+Q_{19}(t, 0)$$

$$P_{11}(t, L_{11})=P_{12}(t, 0)=P_{20}(t, 0)$$

$$Q_{11}(t, L_{11})=Q_{12}(t, 0)+Q_{20}(t, 0)$$

$$P_{12}(t, L_{12})=P_{13}(t, 0)=P_{21}(t, 0)$$

$$Q_{12}(t, L_{12})=Q_{13}(t, 0)+Q_{21}(t, 0)$$

$$P_4(t, L_4)=P_5(t, 0)=P_{14}(t, 0)$$

$$Q_4(t, L_4)=Q_5(t, 0)+Q_{14}(t, 0)$$

$$P_5(t, L_5)=P_6(t, 0)=P_{15}(t, 0)$$

$$Q_5(t, L_5)=Q_6(t, 0)+Q_{15}(t, 0)$$

$$P_6(t, L_9)=P_7(t, 0)=P_{16}(t, 0)$$

$$Q_6(t, L_9)=Q_7(t, 0)+Q_{16}(t, 0)$$

$$P_7(t, L_9)=P_8(t, 0)=P_{17}(t, 0)$$

$$Q_7(t, L_9)=Q_8(t, 0)+Q_{17}(t, 0) \quad (8)$$

The clockwise direction was chosen here as a positive one for loops 2→4→5…8→3 and 2→9→10→...13→3. Substituting (3)-(4) in (8) brings to the nonlinear system for the set of the unknown parameters $\{X_k\}_{k=1}^{33} = \{P_{2-21}^0, \Gamma_{1-13}\}$ of model II determining:

$$P_1^0(1+\Gamma_1)e^{\lambda_1} = P_2^0(1+\Gamma_2 e^{2\lambda_2}) = P_3^0(1+\Gamma_3 e^{2\lambda_3})$$

$$P_2^0(1+\Gamma_2)e^{\lambda_2} = P_4^0(1+\Gamma_4 e^{2\lambda_4}) = P_9^0(1+\Gamma_9 e^{2\lambda_9})$$

$$P_3^0(1+\Gamma_3)e^{\lambda_3} = P_8^0(1+\Gamma_8)e^{\lambda_8} = P_{13}^0(1+\Gamma_{13})e^{\lambda_{13}}$$

$$P_4^0(1+\Gamma_4)e^{\lambda_4} = P_5^0(1+\Gamma_5 e^{2\lambda_5}) = P_{14}^0(1+\Gamma_{14} e^{2\lambda_{14}})$$

$$P_5^0(1+\Gamma_5)e^{\lambda_5} = P_6^0(1+\Gamma_6 e^{2\lambda_6}) = P_{15}^0(1+\Gamma_{15} e^{2\lambda_{15}})$$

$$P_6^0(1+\Gamma_6)e^{\lambda_6} = P_7^0(1+\Gamma_7 e^{2\lambda_7}) = P_{16}^0(1+\Gamma_{16} e^{2\lambda_{16}})$$

$$P_7^0(1+\Gamma_7)e^{\lambda_7} = P_8^0(1+\Gamma_8 e^{2\lambda_8}) = P_{17}^0(1+\Gamma_{17} e^{2\lambda_{17}})$$

$$P_9^0(1+\Gamma_9)e^{\lambda_9} = P_{10}^0(1+\Gamma_{10} e^{2\lambda_{10}}) = P_{18}^0(1+\Gamma_{18} e^{2\lambda_{18}})$$

$$P_{10}^0(1+\Gamma_{10})e^{\lambda_{10}} = P_{11}^0(1+\Gamma_{11} e^{2\lambda_{11}}) = P_{19}^0(1+\Gamma_{19} e^{2\lambda_{19}})$$

$$P_{11}^0(1+\Gamma_{11})e^{\lambda_{11}} = P_{12}^0(1+\Gamma_{12} e^{2\lambda_{12}}) = P_{20}^0(1+\Gamma_{20} e^{2\lambda_{20}})$$

$$P_{12}^0(1+\Gamma_{12})e^{\lambda_{12}} = P_{13}^0(1+\Gamma_{13} e^{2\lambda_{13}}) = P_{21}^0(1+\Gamma_{21} e^{2\lambda_{21}})$$

$$S_1^0(1-\Gamma_1)e^{\lambda_1} = S_2^0(1-\Gamma_2 e^{2\lambda_2}) + S_3^0(1-\Gamma_3 e^{2\lambda_3})$$

$$S_2^0(1-\Gamma_2)e^{\lambda_2} = S_4^0(1-\Gamma_4 e^{2\lambda_4}) + S_9^0(1-\Gamma_9 e^{2\lambda_9})$$

$$S_3^0(1-\Gamma_3)e^{\lambda_3} = S_8^0(1-\Gamma_8)e^{\lambda_8} + S_{13}^0(1-\Gamma_{13})e^{\lambda_{13}}$$

$$S_4^0(1-\Gamma_4)e^{\lambda_4} = S_5^0(1-\Gamma_5 e^{2\lambda_5}) + S_{14}^0(1-\Gamma_{14} e^{2\lambda_{14}})$$

$$S_5^0(1-\Gamma_5)e^{\lambda_5} = S_6^0(1-\Gamma_6 e^{2\lambda_6}) + S_{15}^0(1-\Gamma_{15} e^{2\lambda_{15}})$$

$$S_6^0(1-\Gamma_6)e^{\lambda_6} = S_7^0(1-\Gamma_7 e^{2\lambda_7}) + S_{16}^0(1-\Gamma_{16} e^{2\lambda_{16}})$$

$$S_7^0(1-\Gamma_7)e^{\lambda_7} = S_8^0(1-\Gamma_8 e^{2\lambda_8}) + S_{17}^0(1-\Gamma_{17} e^{2\lambda_{17}})$$

$$S_9^0(1-\Gamma_9)e^{\lambda_9} = S_{10}^0(1-\Gamma_{10} e^{2\lambda_{10}}) + S_{18}^0(1-\Gamma_{18} e^{2\lambda_{18}})$$

$$S_{10}^0(1-\Gamma_{10})e^{\lambda_{10}} = S_{11}^0(1-\Gamma_{11} e^{2\lambda_{11}}) + S_{19}^0(1-\Gamma_{19} e^{2\lambda_{19}})$$

$$S_{11}^0(1-\Gamma_{11})e^{\lambda_{11}} = S_{12}^0(1-\Gamma_{12} e^{2\lambda_{12}}) + S_{20}^0(1-\Gamma_{20} e^{2\lambda_{20}})$$

$$S_{12}^0(1-\Gamma_{12})e^{\lambda_{12}} = S_{13}^0(1-\Gamma_{13} e^{2\lambda_{13}}) + S_{21}^0(1-\Gamma_{21} e^{2\lambda_{21}})$$

where $\lambda_j = -I\omega L_j/c_j$, $S_j^0 = P_j^0 Y_j^0$, j=1–21. This system may be represented in a common form:

$$\{f_j(X_k) = 0\}_{j,k=1}^{33} \tag{9}$$

where $\{f_j\}_{j=1}^{33}$ – the equations in the above system. System (9) was solved numerically by modified Newton's method for nonlinear systems of equations with complex coefficients

$$\boldsymbol{X}_k^{(n+1)} = \boldsymbol{X}_k^{(n)} - \boldsymbol{W}^{-1}(\boldsymbol{X}_k^{(n)}) f(\boldsymbol{X}_k^{(n)}) \tag{10}$$

where $X_k^{(n)}$ the n-th approximation, $W_{lm} = \left| \dfrac{\partial f_l}{\partial X_m} \right|$ – Jacobi matrix. Iterations (10) were provided until a given accuracy of $\{X_k\}_{k=1}^{33}$ calculations was achieved. Then total input admittance of model II was calculated by substituting the obtained value Γ_1 in (5).

V. RESULTS AND DISCUSSION

The input admittance for the models I and II was calculated at the variation of the parameters Y_i^t that reflect normal or pathological state of the microcirculation of the inner organ; parameters a, ξ, R_1, that reflect the geometry of the intraorganic vasculature; parameters E_i, R_i, μ, χ, that reflect the mechanical properties of the vasculature which may also be modified by pathological processes. In connection with the significant effect of the length of the feeding artery on the set of the resonant harmonics of the organ (Wang *et al*., 2000b), the influence of variation L_1 on the input admittance was investigated separately. For the viscous properties of the vascular wall modeling the empirical relations $\theta_i = \theta_i^0(1-e^{-\lambda\omega})$, $\theta_i^0 = \chi 10 h_i/D_i$ where $\chi = const$ (Milnor, 1989; Taylor, 1966; Karamanoglu *et al*., 1995) were used.

The average values for the parameters were taken as ρ=1050 kg/m^3, μ=4.5×10^{-3} Pa·s, σ=0.4, R_1=0.002 m, χ=5–15°, λ=2; a=2.6–7.59, b=1 according to (Dawson *et al*., 1999), E_i=(6–10)×10^5 Pa and E_i=(1–2.5)×10^6 Pa for elastic and muscle arteries. The statistical dependences $E_i(R_i)$ and $h_i(R_i)$ (Avolio, 1980; Karamanoglu *et al*., 1995) were used as well.

Significant variation of arterial input impedance can occur either in the course of normal physiological responses of the circulation to different factors or in connection with pathologically changed parameters of the circulatory and/or regulatory systems (Milnor, 1989). The principal mechanism of physiological (normal) changes is connected with the alterations of the smooth muscle in the arterial wall activity, that causes the simultaneous variations in E_i, R_i, σ and, thus in Y_i^0, c_i. The basic normal changes in hemodynamics of an inner organ are connected with its activity, that is influenced by active work, digestion, etc. These variations are well-known and taken into account in traditional Chinese pulse diagnosis (Hammer, 2001; Wang, 1997; Flaws, 1997). This kind of normal activity is determined by multivariant changes in E_i, R_i, σ and microcirculation, i.e. by Re(Y_i^t) and Im(Y_i^t). For definiteness the values Y_i^t were considered as $Y_i^t = Y_{i+7}^0(y+iz)$, y, $z \in [0, 1]$, i=1–8, where y=Re(Y_i^t)/Y_{i+7}^0, z=Im(Y_i^t)/Y_{i+7}^0. In this way each terminal admittance was determined by its last-order artery and might produce the corresponding backward wave at $\Gamma_i \in [0, 1]$. Dilation or constriction of arterioles changes the peripheral reflection coefficient and, thus modifies the input admittance spectrum. Diminishing Re(Y_i^t) enlarges the reflection coefficients and increases the depth of the minima and the height of the maxima of the $Y_1(\omega)$.

Any changes in R_i produce changes in the characteristic admittance Y_i^0 of the corresponding vessel and pulse wave velocity. In the case of $h_i/R_i = const$ the wave velocity is a monotonous increasing function of R_i. Actually for different arteries the value h_i/R_i=0.12–0.52 (Karamanoglu *et al*., 1995) and the dependence $h_i/R_i(R_i)$ can be approximated by hyperbola. In this case the dependence $c_i(R_i)$ becomes non-monotonous.

Assuming slight monotonous increasing E_i and decreasing h_i with R_i based on the data (Milnor, 1989; Karamanoglu *et al*., 1995), the next results were obtained for the model I. At first, the tree geometry defines the resonant harmonics, as they were introduced in (Wang *et al*., 1991; Yu *et al*., 1994; Lu *et al*., 1996; Young *et al*., 1992; Wang *et al*., 2000a; Wang *et al*., 2000b), and their amplitudes. The influence of the branching asymmetry ξ=0.25–1 on $Y_1^\circ = Y_1/$

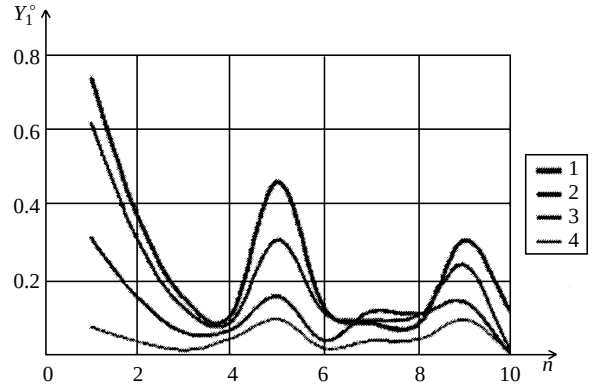

Fig. 2 Effect of branching asymmetry ξ on the input admittance of model I. Numbers 1–4 correspond to ξ=0.25–1 in steps of 0.25

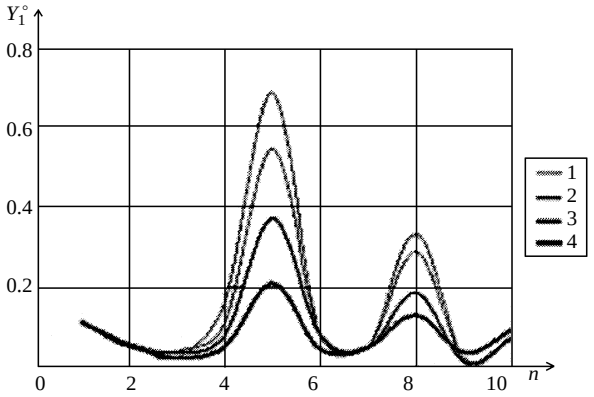

Fig. 4 Effect of decreased R_2 (R_2=1.6;0.8;0.4;0.2 mm, curves 4–1 respectively) on input admittance of model I, asymmetrical branching at ξ=0.7, R_1=2.5 mm

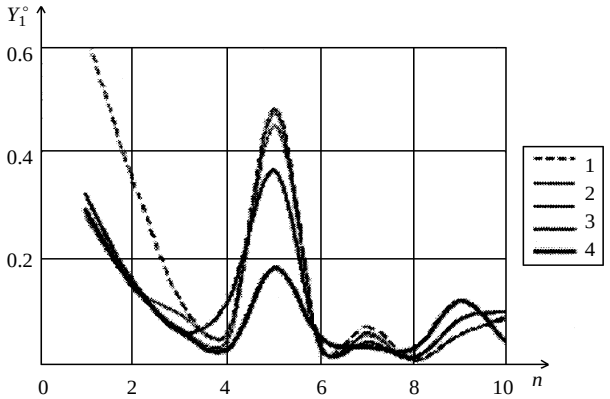

Fig. 3 Effect of decreased R_2 (R_2=2;1;0.5;0.25;0.12 mm, curves 5–1 respectively) on input admittance of model I, symmetrical branching at ξ=1, R_1=2.5 mm

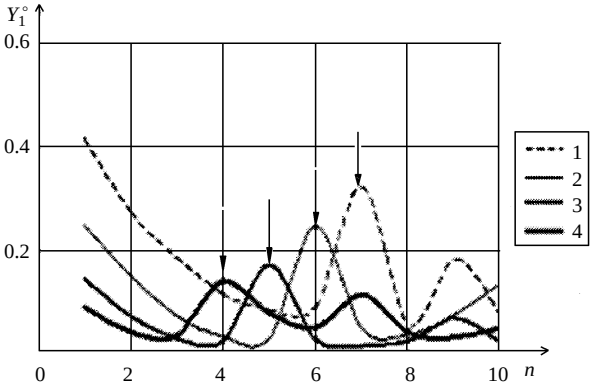

Fig. 5 Effect of increased a on the main resonant harmonics (indicated by arrows) in the self-similar tree (model I) with $L_i=aR_i$, R_1=2.5 mm. Numbers 1–4 correspond to a=5–12.5 in steps of 2.5

Y_1^0 is shown in Fig. 2. The corresponding values $Y_1|_{\omega=0}$ are not pointed out at the figures because they should be calculated separately for a steady flow problem. Direct substitution ω=0 in (5)-(7), (9) gives the values $Y_1|_{\omega=0}\sim\mathrm{Re}(Y_{1-8}^t)$ and $Y_1|_{\omega=0}<<Y_1|_{\omega=2\pi}$ that are small in comparison with the Y_1. The value ξ=1 corresponds to a completely symmetric arterial tree that matches the vasculature of some inner organs (Zamir, 2001). The asymmetric branching with ξ=0.25–0.5 produces two kinds of vessels: the larger distributing vessels and the smaller delivering ones (Zamir and Phipps, 1987; Zamir and Shee, 1987). The set of resonant harmonics are quite similar for the trees with different ξ (Fig. 2) and correspond to the first maxima and minima of $Y_1(n)$, where n - the number of harmonics. This result is coordinated with the model of the asymmetrically branching tree with $i>20$ orders of branching (Bondarenko and Kizilova, 2002). The changes in the diameters of one of the second-order tubes R_2 or R_3 cause the variations in the amplitudes of the resonant harmonics and, progressively diminish the corresponding R_i, the significant changes in the amplitudes of the additional harmonics (Figs. 3-4). In the case of the asymmetric tree the contraction of the larger artery in the bifurcation has more significant effect on the amplitudes of the resonant harmonics.

The length of the feeding artery as well as the lengths of the self-similar tree define the set of resonant harmonics. The increasing of a in the self-similar tree with $L_i=aR_i$ shifts the main resonant harmonics to the lower frequencies (Fig. 5). The same result is obtained for the self-similar trees (Brown, 1996; Bondarenko and Kizilova, 2002). The independent increasing of the length L_1 for a given downstream vasculature produces the shift of the main resonant harmonics to the lower frequencies. For certain limits of L_1 variations the set of resonant harmonics remains the same and is defined by the similarity parameter a of the tree only. For instance, for the parameters' values that were used for calculations of the curves in Fig. 5, $L_1\in[1.5, 5]$ cm corresponds to n=7, 8, $L_1\in[5, 12.5]$ cm – n=5, 6, $L_1\in[12.5, 20]$ cm

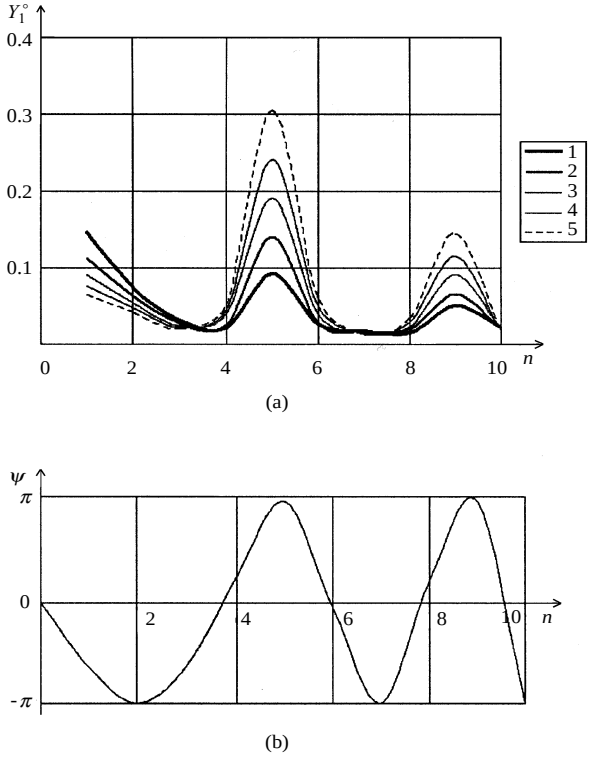

Fig. 6 (a) Effect of $\mathrm{Re}(Y_i^t)$ increasing on the amplitudes of the resonant harmonics (n=5; 9) of the model I, symmetrical branching. Curves 1–5 correspond to $\mathrm{Re}(Y_i^t)$=0–1 in steps of 0.25 at $\mathrm{Im}(Y_i^t)$=0.5; (b) Phases of the input admittance of the model I, symmetrical branching. Maxima and minima of $\psi(n)$ correspond to extremes of $Y_1(n)$

– n=3, 4 harmonics of the pulse wave. Hence it follows that the length L_1 of the feeding artery defines the set of resonant harmonics of a given organ. This conclusion corresponds to the experimental and theoretical investigations (Wang *et al.*, 2000b). Besides some individual variations in L_1 do not change this set providing the possibility of pulse diagnosis of the organ state without preliminary knowledge of the individual vasculature of the organ.

The pathological changes in hemodynamics of the organ evoke certain changes in Y_i^t. Arteriolar vasoconstriction/vasodilation cause variations in the cross-sectional area of the vessels and wall stiffness that decrease/ increase $\mathrm{Re}(Y_i^t)$, $\mathrm{Im}(Y_i^t)$. The influence of $\mathrm{Re}(Y_i^t)$, $\mathrm{Im}(Y_i^t)$ variations on the input admittance spectrum is illustrated in Figs. 6a-b. The $\mathrm{Re}(Y_i^t)$ decreasing at a constant $\mathrm{Im}(Y_i^t)$ led to some variations in the amplitude of the first and second maxima of the $Y_1(n)$ (Fig. 6a) at the expense of the backward pulse wave amplitude increasing. The phase spectrum remains invariable and reaches maxima and minima at the resonant harmonics (Fig. 6b) according to (Yu *et al.*, 1994). The $\mathrm{Im}(Y_i^t)$ decreasing at a constant $\mathrm{Re}(Y_i^t)$ significantly changes the

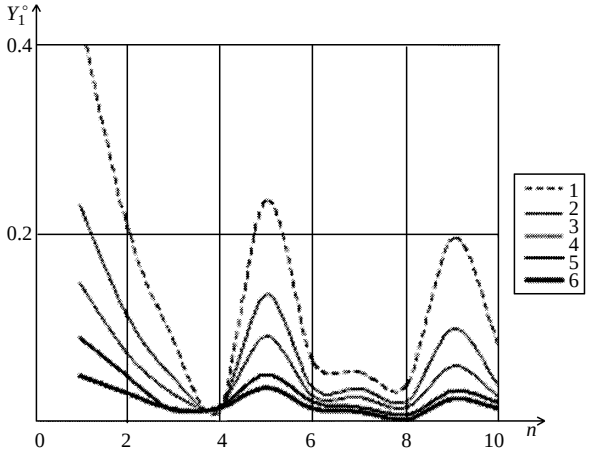

Fig. 7 Effect of increased blood viscosity μ on the input admittance of model I, asymmetrical branching at ξ=0.8. Numbers 1–5 correspond to μ=(1.7;3;4.5;10;22.5)·10^{-3} Pa·s, curve 3 – normal viscosity, curves 1 and 5 – maximally registered pathological decreasing and increasing of blood viscosity

phase spectrum and slightly changes the amplitudes of the resonant harmonics. Simultaneous variations of $\mathrm{Re}(Y_i^t)$, $\mathrm{Im}(Y_i^t)$ cause the same changes in $Y_1(n)$. All the changes are practically equivalent for the microcirculatory system uniformity (Y_i^t=Y^t, i=1–8) or non-uniformity ($Y_i^t \neq Y_k^t$, i, k=1–8). The last case corresponds to possible pathological asymmetry in the distribution of contracted/dilated arterioles, working capillaries, their elastic properties, etc.

The Young's modulus and the blood viscosity variations within wide limits cause the same changes in the amplitudes of certain sets of harmonics mainly. The blood viscosity pathological decrease/increase evokes the corresponding changes in the maxima $Y_1^\circ(n)$ (Fig. 7).

These changes are counter to the ones connected with R_i variations according to Womersley's number expression – the only one containing μ. The most noticeable changes in $Y_1^\circ(n)$ are observed for the second and third maxima $Y_1^\circ(n)$. The Young's modulus decreasing/increasing within two-orders limits cause not only the amplitudes changing but some shift of the $Y_1^\circ(n)$ to the lower/higher harmonics respectively as well (Fig. 8). These results completely agree with the calculations on T-tube model (Liu *et al.*, 1989).

Hence it follows that different multidirectional changes in the microcirculatory system evoke the similar changes in the amplitude and phase spectra of the input admittance of the inner organ with a given vasculature and these changes can not be distinguished and interpreted in the frames of the medical diagnostics. Mathematically it means the non-uniqueness of the inverse hemodynamic problem solution.

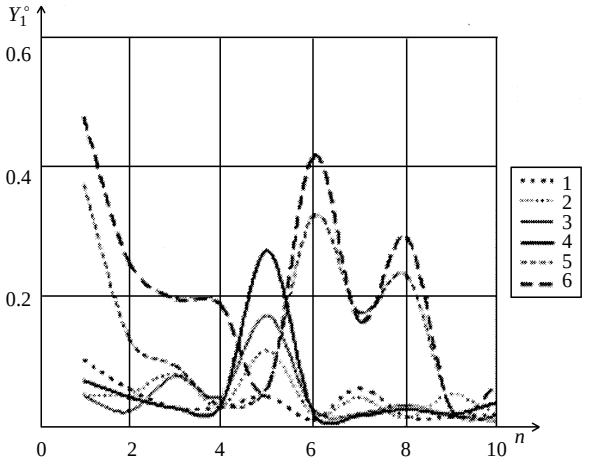

Fig. 8 Influence of increased E_i in each vessel on the input admittance of model I, asymmetrical branching at ξ=0.6. Numbers 1–6 correspond to E=(0.5; 1;5; 10; 50; 100)·10^5 Pa

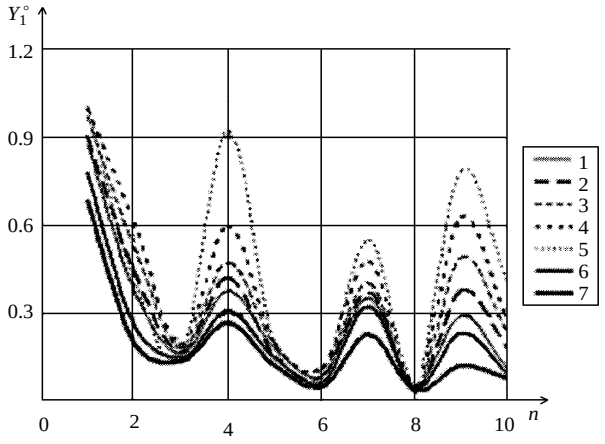

Fig. 9 Effect of Re(Y_i^t) increasing on the amplitudes of the resonant harmonics (n=4; 7; 9) of the model II, symmetrical branching. Curves 1–7 correspond to Re(Y_i^t)=0–1 in steps of 0.25 at Im(Y_i^t)=0.5 and Im(Y_i^t)=0;1 at Re(Y_i^t)=0.1 respectively

The infinite number of solutions to the inverse problem of the pulse wave propagation in multibranched system was already discussed as applied to the tree geometry identification (Quick *et al.*, 2001). Nevertheless the pathological changes connected with blood congestion, systemic pressure, arterial stiffness and smooth muscle activity increasing, tissue (interstitial) pressure increase finally promotes Y_i^t decrease. These changes can be easily discovered by increase of the resonant harmonics amplitudes. On the other hand this sort of change can be attributed to the so-called excess syndrome of oriental medicine. The opposite pathological changes that can be attributed in total to the deficiency syndrome evoke decreasing of the correspondent amplitudes. In that way the diagnostics of the pathology state of the organ with known set of the resonant harmonics can be conducted in excess/deficiency terms unambiguously. The resonant harmonics amplitudes increase/decrease monotonically coupled with the excess factor intensity increase/decrease. It helps to conduct the interpretation of $Y_1^\circ(n)$ curves in excess/deficiency terms without detailed understanding of the correspondent pathological variations of all the hemodynamical parameters. It should be pointed out that the diagnostics of the combined pathologies of different inner organs by the resonant harmonics method (Wang *et al.*, 1991; Yu *et al.*, 1994; Lu *et al.*, 1996; Young *et al.*, 1992; Wang *et al.*, 2000a; Wang *et al.*, 2000b) remains unclear. Different organs possess quite different main and some additional resonant harmonics (Yu *et al.*, 1994; Lu *et al.*, 1996; Wang *et al.*, 2000a) and the coincidence of main and additional harmonics of different organs would be expected.

The main difference of the model II as compared

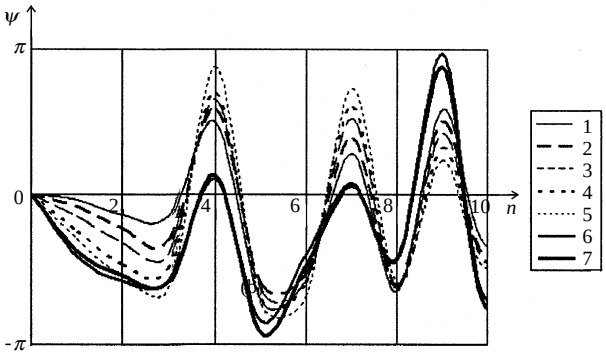

Fig. 10 The phase of the input admittance of the model II, symmetrical branching. Curves 1–7 correspond to the same cases as in Fig. 9

to the model I consists in the resonant harmonics set widening and their amplitudes significantly changing in response to the Y_i^0, c_i, Y_i^t changes. The set is completely defined by the length of the feeding artery L_1 and the anastomoses location. Compared to the model I and single anastomos model (Kizilova, 2002) model II possesses additional resonant harmonics at high frequencies (Figs. 9-10). The amplitudes of the additional harmonics exhibit the most noticeable variation in response to the pathological changes of Y_i^t (Fig. 9), R_i (Fig. 11), E_i (Fig. 12) that are accompanied by regular changes of a phase spectrum with well defined extremes (Fig. 10). The sharpening of $Y_1^\circ(n)$ curves at some points for the model II as compared with the model I is connected with additional backward waves moving through tube 1 by the routes 1→2→4...→8→3→1 and 1→3→8...→4→2→1. The phases of the additional waves

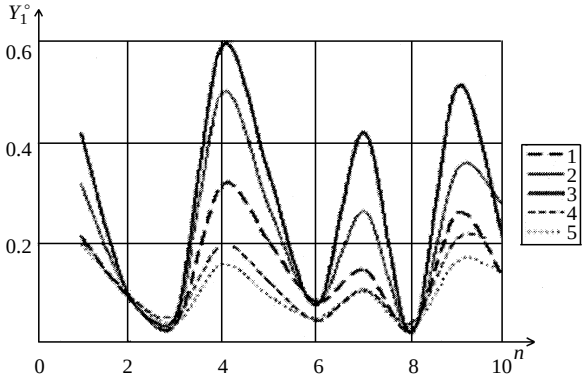

Fig. 11 Effect of R_2 variation on input admittance of model II at ξ=1, R_1=2.5 mm. (R_2=0.2; 0.8; 1.4; 2.0; 2.6 mm, curves 1–5 respectively)

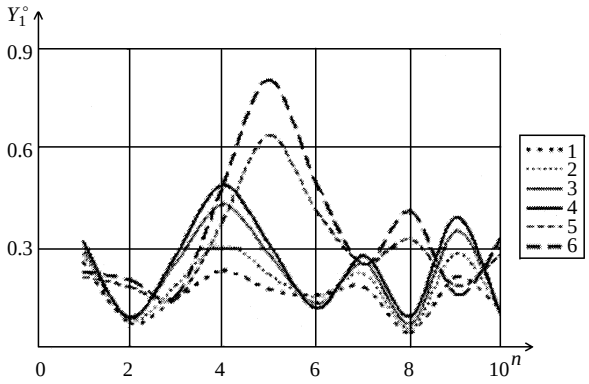

Fig. 12 Influence of increased E_i in each vessel on the input admittance of model II, ξ=0.9. Numbers 1–6 correspond to E=(0.5; 1; 5; 10; 50; 100)·10^5 Pa

depend on the interrelation between the pulse wave rate and the total length of the route. In connection with the dependence $c_i(\omega)$ the correspondent phases depend on the harmonics number. For the symmetrical branching (ξ=1) the noticeable regularity in phase changing is observed for wide variations in $\mathrm{Re}(Y_i^t)$ and $\mathrm{Im}(Y_i^t)$. The independent variations in different terminations Y_i^t, i=1–8 evoke the same remarkable sharpening of $Y_1^\circ(n)$ and $\psi(n)$ at a certain number of harmonics. By contrast, the phase spectrum $\psi(n)$ of the model I does not exhibit such regular changing at variation of the geometrical and mechanical parameters of the model.

The relative independence of the set of the resonant harmonics from some variations in the vascular geometry means the possibility of the pulse wave diagnosis based on the Fourier spectrum analysis of the pressure wave in a peripheral superficial artery. Based on the clinical observations and experiments the correspondence between the main resonant harmonics and the inner organs was proposed. In this scheme n=0–7 correspond to the heart, liver, kidneys, spleen, lung, stomach, gall and urinary bladders (Wang *et al*., 1991; Yu *et al*., 1994; Lu *et al*., 1996; Young *et al*., 1992; Wang *et al*., 2000a). These are the main inner organs and their state can be estimated by the pulse diagnosis methods of traditional Chinese medicine. In light of the experiments (Wang *et al*., 1991; Yu *et al*., 1994; Lu *et al*., 1996) and theoretical modeling (Wang *et al*., 2000b) that implies the progressive diminishing of the feeding arteries of the cited organs. The total morphometric data do not confirm this conclusion. The other way is connected with the differences between the input admittances of the vasculatures with different topology (Bondarenko and Kizilova, 2002; Duan and Zamir, 1993; Kizilova, 2002). Both variations in the L_1 of different organs' vasculature and in the number and order of anastomoses take place in real organs of different patients. In that way the pulse wave propagation and reflection in the systems with anastomoses should be investigated being based on the exact morphometric data of different organs. The infinite number of solutions to the hemodynamic inverse problem (Quick *et al*., 2001) calls into question the analysis of the input admittance spectra for the purpose of medical diagnosis. Nevertheless the method is used in clinics (Lu *et al*., 1996; Wang *et al*., 2000a) and the combination of some geometrical properties (L_1, a, the number and the branching order of the anastomoses) can give the unique set of the resonant harmonics for each organ within the limits of some individual variations. It should be noted that the possibility of the differential diagnostics of the combined pathologies of the inner organs is not clear in the frameworks of the method. The results of the present study confirm the influence of the wide number of pathologically changed parameters of the models on the resonant frequencies of the input admittance. These changes are unlikely to be recognizable in the terms of traditional medicine. At the same time all the changes can be interpreted in terms of excess-deficiency in oriental medicine.

NOMENCLATURE

a	antilog of intercept of $\log(L_i)$ vs. $\log(D_i)$
b	slope of $\log(L_i)$ vs. $\log(D_i)$
c_i	pulse wave velocity in the tube number i, m/s
D_i	diameter of the tube number i, m/s
E_i	Young's modulus of elasticity of vessel's wall material, Pa
h_i	wall thickness of the tube number i, m
L_i	length of the tube number i, m
P_i	intravascular pressure in the tube number i, Pa
P_f, P_b	amplitudes of forward and backward waves, Pa

P_i^0 pressure in the initial cross-section of the tube number i, Pa
Q_i volumetric rate in the tube number i, m^3/s
R_i radius of the tube number i, m
Y_i^t complex terminate admittance of the tube number i, m^4s/kg
$Y_i^/$ complex admittance of the tube number i with its termination, m^4s/kg
Y_i° dimensionless admittance of the tube number i
γ coefficient in Murray's law
Γ_i reflection coefficient at the distal cross-section of the tube number i
ζ asymmetry of the lengths of daughter vessels in a bifurcation
θ_i dimensionless wall viscosity for the tube number i
μ fluid viscosity, Pa·s
ξ asymmetry of the diameters of daughter vessels in a bifurcation
ρ fluid density, kg/m^3
σ_i Poisson's ratio for the vessel wall
ω angular frequency, s^{-1}

REFERENCES

Aharinejad, S., Schreiner, W., and Neumann, F., 1998, "Morphometry of Human Coronary Arterial Trees," *Anatomical Record*, Vol. 251, No. 1, pp. 50-59.

Avolio, A. P.,1980, "Multi-branched Model of the Human Arterial System," *Medical & Biological Engineering and Computing*, Vol. 18, No. 6, pp. 709-718.

Bennett, S. H., Goetzman, B. W., Milstein, J. M., and Pannu, J. S.,1996, "Role of Arterial Design on Pulse Wave Reflection in a Fractal Pulmonary Network," *Journal of Applied Physiology*, Vol. 80, No. 3, pp. 1033-1056.

Bondarenko, M. Y., and Kizilova, N. N., 2002, "Pulse Wave Reflections in Asymmetrically Branching Arterial Networks," *Russian Journal of Biomechanics*, No. 4, pp. 36-49.

Brown, D. J., 1996, "Input Impedance and Reflection Coefficient in Fractal-like Models of Asymmetrically Branching Compliant Tubes," *IEEE Transactions on Biomedical Engineering*, Vol. 43, No. 7, pp. 715-722.

Cross, S. S., Start, R. D., Stephenson, T. J., Cotton, D. W., Variend, S., and Underwood, J. C., 1995, "Fractal Geometric Analysis of the Renal Arterial Tree in Infants and Fetuses," *Pediatric Pathology and Laboratory Medicine*, Vol. 15, No. 2, pp. 259-268.

Dawson, C. A., Krenz, G. S., Karau, K. L., Haworth, S. T., Hanger, C. C., and Linehan, J. H., 1999, "Structure-function Relationships in the Pulmonary Arterial Tree," *Journal of Applied Physiology*, Vol. 86, No. 2, pp. 569-583.

Duan, B., and Zamir, M., 1993, "Reflection Coefficients in Pulsatile Flow through Converging Junctions and the Pressure Distribution in a Simple Loop," *Journal of Biomechanics*, Vol. 26, No. 12, pp. 1439-1447.

Flaws, B., 1997, *The Secret of Chinese Pulse Diagnosis*, Blue Poppy Press, Boulder, CO, USA.

Gan, R. Z., Tian, Y., Yen, R. T., and Kassab, G. S., 1993, "Morphometry of the Dog Pulmonary Venous Tree," *Journal of Applied Physiology*, Vol. 75, No. 1, pp. 432-440.

Gil-Garcia, J., Gimeno-Dominguez, M., and Murillo-Ferroll, N. L., 1992, "The Arterial Pattern and Fractal Dimension of the Dog Kidney," *Histology and Histopathology*, Vol. 7, No. 4, pp. 563-574.

Hammer, L., 2001, *Chinese Pulse Diagnosis: A Contemporary Approach*. Eastland Press, Seattle, WA, USA.

Huang, W., Yen, R. T., Mclaurine, M., and Bledsoe, G., 1996, "Morphometry of the Human Pulmonary Vasculature," *Journal of Applied Physiology*, Vol. 81, No. 5, pp. 2123-2133.

Karamanoglu, M., Gallacher, D. E., Avolio, A. P., and O'Rourk, M. F., 1995, "Pressure Wave Propagation in a Multibranched Model of the Human Upper Limb," *American Journal of Physiology*, Vol. 269, No. 4, Part 2, pp. H1363-H1369.

Kizilova, N. N., 2002, "Pulse Wave Reflections and Resonant Properties of Arterial Beds with Anastomoses," *Mathematical Modeling*, Vol. 14, No. 5, pp. 115-121.

Liu, Z. R., Shen, F., and Yin, F. C., 1989, "Impedance of Arterial System Simulated by Viscoelastic T-tubes Terminated in Windkessels," *American Journal of Physiology*, Vol. 256, No. 4, Part 2, pp. H1087-H1099.

Lu, W. A., Cheng, C. H., Lin Wang, Y. Y., and Wang, W. K., 1996, "Pulse Spectrum Analysis of Hospital Patients with Possible Liver Problems," *American Journal of Chinese Medicine*, Vol. 24, No. 3-4, pp. 315-320.

Milnor, W. R., 1989, *Hemodynamics*, Williams &Wilkins, Baltimore, MD, USA.

Quick, Ch. M., Young, W. L., and Noordegraaf, A., 2001, "Infinite Number of Solutions to the Hemodynamic Inverse Problem," *American Journal of Physiology*, Vol. 280, No. 4, pp. H1472-H1479.

Reuderink, P. J., Hoogstraten, H. W., and Sipkema, P., 1989, "Linear and Nonlinear One-dimentional Models of Pulse Wave Transmission at High Womersley Numbers," *Journal of Biomechanics*, Vol. 22, No. 12, pp. 819-827.

Stergiopulos, N., Meister, J.-J., and Westerhof, N.,

1995, "Scatter in Input Impedance Spectrum May Result from the Elastic Nonlinearity of the Arterial Wall," *American Journal of Physiology*, Vol. 269, No. 4, Part 2, pp. H1490-H1495.

Taylor, M. G., 1966, "The Input Impedance of an Assembly of Randomly Branching Elastic Tubes," *Biophiysical Journal*, Vol. 6, No. 1, pp. 29-51.

Wang, S. H., 1997, *The Pulse Classic: A Translation of the Mai Jing by Wan S. H.*, Blue Poppy Press, Boulder, CO, USA.

Wang, W. K., Bau, J. G., Hsu, T. L., and Wang, Y. Y., 2000a, "Influence of Spleen Meridian Herbs on the Harmonic Spectrum of the Arterial Pulse," *American Journal of Chinese Medicine*, Vol. 28, No. 2, pp. 279-289.

Wang, Y. Y., Chang, S. L., Wu, Y. E., Hsu, T. L., and Wang, W. K., 1991, "Resonance. The Missing Phenomenon in Hemodynamics," *Circulation Research*, Vol. 69, No. 1, pp. 246-249.

Wang, Y. Y., Lia, W. C., Hsiu, H., Jan, M. Y., and Wang, W. K., 2000b, "Effect of Length on the Fundamental Resonance Frequency of Arterial Models Having Radial Dilatation," *IEEE Transactions on Biomedical Engineering*, Vol. 47, No. 3, pp. 313-318.

Womersley, J. R., 1957, "An Elastic Tube Theory of Pulse Transmission and Oscillatory Flow in Mammalian Arteries," *Technical Report TR-56-614*.

Young, S. T., Wang, W. K., Chang, L. S., and Kuo, T. S., 1992, "The Filter Properties of the Arterial Beds of Organs in Rats," *Acta Physiologica Scandinavica*, Vol. 145, No. 4, pp. 401-406.

Yu, G. L., Wang, Y. L., and Wang, W. K., 1994, "Resonance in the Kidney System of Rats, " *American Journal of Physiology*, Vol. 267, No. 4, Part 2, pp. H1544-H1548.

Zamir, M., 1998, "Mechanics of Blood Supply to the Heart: Wave Refection Effects in a Right Coronary Artery," *Proceedings of the Royal Society of London, Series B: Biological Sciences*, Vol. 265, No. 1394, pp. 439-444.

Zamir, M., 2001, "Arterial Branching within the Confines of Fractal L-System Formalism," *Journal of General Physiology*, Vol. 118, No. 3, pp. 267-275.

Zamir, M., and Phipps, S., 1987, "Morphometric Analysis of the Distributing Vessels of the Kidney," *Canadian Journal of Physiology and Pharmacology*, Vol. 65, No. 12, pp. 2433-2440.

Zamir, M., and Shee, H., 1985, "Branchimg Characteristics of Human Coronary Arteries," *Canadian Journal of Physiology and Pharmacology*, Vol. 64, No. 6., pp. 661-668.

Zamir, M., and Shee, H., 1987, "Segment Analysis of Human Coronary Arteries," *Blood Vessels*, Vol. 24, No. 1-2, pp. 76-87.

Manuscript Received: Jan. 08, 2003
Revision Received: May 03, 2003
and Accepted: Jul. 18, 2003